



On the Role of a Conserved Methionine in the Na⁺-Coupling Mechanism of a Neurotransmitter Transporter Homolog

Wenchang Zhou¹ · Gianluca Trinco² · Dirk J. Slotboom² · Lucy R. Forrest³ · José D. Faraldo-Gómez¹

Received: 13 November 2020 / Revised: 17 January 2021 / Accepted: 19 January 2021 / Published online: 9 February 2021
© The Author(s) 2021

Abstract

Excitatory amino acid transporters (EAAT) play a key role in glutamatergic synaptic communication. Driven by transmembrane cation gradients, these transporters catalyze the reuptake of glutamate from the synaptic cleft once this neurotransmitter has been utilized for signaling. Two decades ago, pioneering studies in the Kanner lab identified a conserved methionine within the transmembrane domain as key for substrate turnover rate and specificity; later structural work, particularly for the prokaryotic homologs Glt_{ph} and Glt_{Tk}, revealed that this methionine is involved in the coordination of one of the three Na⁺ ions that are co-transported with the substrate. Albeit extremely atypical, the existence of this interaction is consistent with biophysical analyses of Glt_{ph} showing that mutations of this methionine diminish the binding cooperativity between substrates and Na⁺. It has been unclear, however, whether this intriguing methionine influences the thermodynamics of the transport reaction, i.e., its substrate:ion stoichiometry, or whether it simply fosters a specific kinetics in the binding reaction, which, while influential for the turnover rate, do not fundamentally explain the ion-coupling mechanism of this class of transporters. Here, studies of Glt_{Tk} using experimental and computational methods independently arrive at the conclusion that the latter hypothesis is the most plausible, and lay the groundwork for future efforts to uncover the underlying mechanism.

Keywords Transport stoichiometry · Molecular dynamics simulations · Cation-methionine interactions · Sulfur polarization

Special Issue: In Honor of Prof. Baruch Kanner.

Wenchang Zhou and Gianluca Trinco have contributed equally to this work.

-
- ✉ Dirk J. Slotboom
d.j.slotboom@rug.nl
 - ✉ Lucy R. Forrest
lucy.forrest@nih.gov
 - ✉ José D. Faraldo-Gómez
jose.faraldo@nih.gov

¹ Theoretical Molecular Biophysics Laboratory, National Heart, Lung and Blood Institute, National Institutes of Health, Bethesda, MD 20892, USA

² Groningen Biomolecular Sciences and Biotechnology Institute, Zernike Institute for Advanced Materials, University of Groningen, Groningen, The Netherlands

³ Computational Structural Biology Section, National Institute of Neurological Disorders and Stroke, National Institutes of Health, Bethesda, MD 20892, USA

Introduction

Glutamatergic synapses are the primary excitatory synapses in the brain and are thought to be essential for learning and memory. In this form of chemical signaling, glutamate is released by the presynaptic nerve terminal, activating receptor proteins on the surface of the post-synaptic neuron. Excessive quantities of glutamate in the synaptic cleft, however, can be cytotoxic and are associated with traumatic events such as stroke (reviewed in [1, 2]). Reuptake of glutamate is thus key to maintaining healthy levels, a task that falls largely to membrane transporters belonging to the SLC1 family, also known as excitatory amino acid transporters (EAAT) in the transporter classification database (TCDB) family 2.A.23 [3, 4]. Structures of prokaryotic SLC1 homologues, including Glt_{ph} and Glt_{Tk}, from *Pyrococcus horikoshii* and *Thermococcus kodakarensis*, respectively [5–7], and of a thermally-stabilized mutant of EAAT1 (SLC1A1 or GLAST) [8], reveal a trimeric assembly, where each protomer contains eight transmembrane (TM) segments and two helical hairpins, HP1 and HP2. The three protomers interact through their so-called trimerization domains

(Fig. 1a), whose relative orientation remains constant during transport [9]. By contrast, the substrate-binding transport domains, in the periphery of the complex, (Fig. 1a) undergo dramatic conformational changes, often referred to as elevator-like movements, in order to allow alternating access to the binding sites from each side of the membrane [10–14].

Like their mammalian cousins, Glt_{ph} and Glt_{Tk} both require three sodium ions to drive transport of the substrate dicarboxylic acid [15–18]. However, they also differ in that they have a higher affinity for L-aspartate than for L-glutamate, and do not require antiport of potassium nor co-transport of a proton [5, 19, 20]. The binding sites for sodium and substrate are buried beneath HP2 in the core of the transport domain, and in close proximity to one another (Fig. 1b, c) but not in direct contact. The Na^+ binding site furthest from the extracellular surface of the protein, denominated Na3, is formed by Tyr91, Thr94 and Ser95 in TM3 (residue numbering in Glt_{Tk} will be used hereafter) as well as Asn313 and Asp315 from TM7 (Fig. 1c). The latter are part of a conserved sequence motif, NMDGT, which the Kanner lab revealed to be essential for the transport functionality of mammalian transporters [21–24]. Asn313 also contributes a backbone carbonyl atom to the so-called Na1 site, as does Gly309 from TM7, the side chain of Asp409, and the backbone carbonyl of Asn405, both in TM8 (Fig. 1c). The Na2 site is the most proximal to the extracellular space, and also to the substrate binding site. Ion coordination at this site differs from that of Na1 and Na3, in that it does not involve a direct contact with an acidic sidechain, as is typical among Na^+ -coupled transporters [25–29]. Instead, it involves only four backbone carbonyl oxygens from residues in HP2 (Ser352, Ile353 and Thr355) and TM7 (Thr311), and most strikingly, the sidechain of Met314, of the NMDGT motif (Fig. 1b).

This methionine is particularly intriguing. In the known EAAT structures, it separates the Na^+ ion in the Na2 site from the substrate, when both are bound. However, such direct methionine- Na^+ contacts are extraordinarily rare: a search of the Protein Data Bank [30] reveals only three other structures that appear to feature this interaction, but none of those proteins are known to be Na^+ dependent, so these assignments are not conclusive (Table S1). Yet Met314 is conserved in all known sodium-coupled transporters in the SLC1 family; interestingly, though, it is substituted by Leu in proton-coupled transporters such as *E. coli* GltP [31] and *B. subtilis* DctA [32]. Studies in the Kanner lab have examined the effects resulting from mutation of this conserved methionine in Na^+ -dependent mammalian transporters (Met397 in EAAT2, SLC1A2 or GLT-1, and Met367 in EAAT3, SLC1A3 or EAAC1). Interestingly, substitutions by Cys, Leu, Ala or Ser were observed to severely diminish

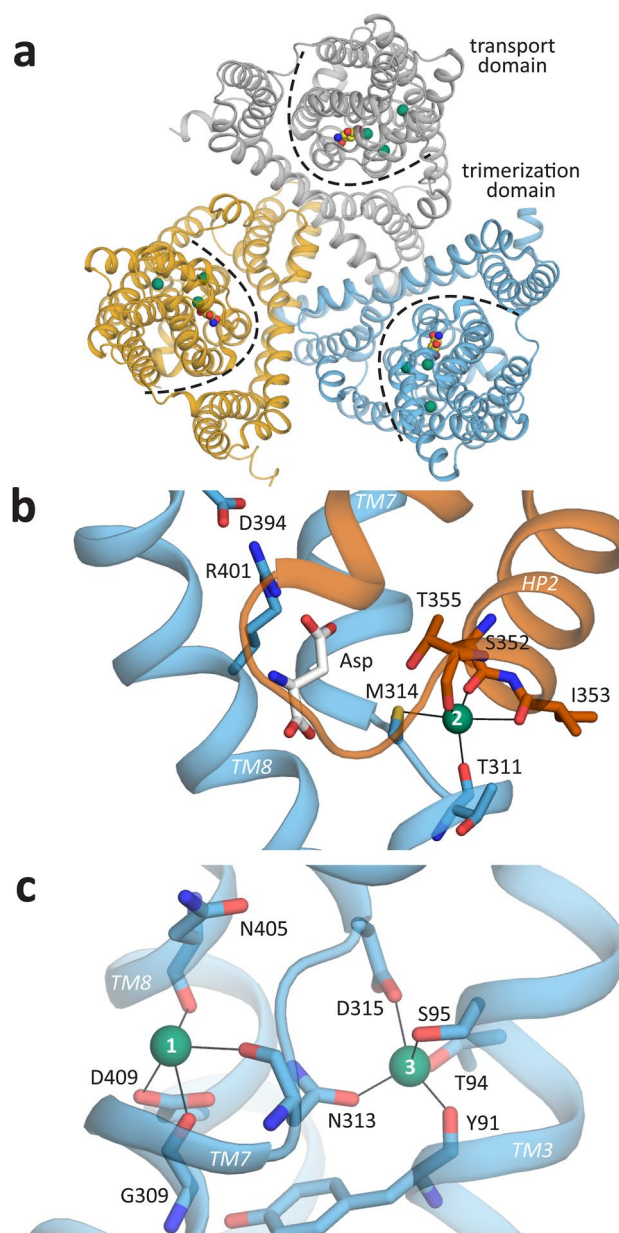


Fig. 1 Structure and binding sites of Glt_{Tk} . **a** The structure of the holo trimer (PDB entry 5E9S), in an outward-facing conformation, is viewed from the extracellular side and shown as cartoon helices, with each subunit in a different color. Dashed lines indicate the boundaries between the transport domain and trimerization domain in each protomer. Sodium ions (green) and L-aspartate (yellow, blue and red) are shown as spheres. **b** Close-up view of the binding site for L-aspartate (sticks with carbon atoms in white), and of the Na^+ binding site referred to as Na2 (green sphere), with key residues, including Met314, shown as sticks and labelled. Hairpin HP2 (orange) occludes access to these sites from the extracellular side. Thin black lines indicate oxygen- or sulfur-ion coordination. **c** Close-up of the Na1 and Na3 sites, deeper into the structure of the transport domain, showing key residues involved in Na^+ coordination

the rate of substrate uptake and to alter its dependence on Na^+ concentration [21, 23, 33], in a manner that suggests Na^+ binding is partially impaired. For example, for Cys, Ser and Leu substitutions, Na^+ -driven uptake of L-[^3H]-glutamate and D-[^3H]-aspartate was reduced relative to the wild type transporter by 10–20-fold, reflecting concomitant changes in K_m measured using steady-state transport currents [33]. Moreover, the $K_{0.5}$ for Na^+ required to activate those steady-state currents was increased by at least 2.5-fold relative to the wild type transporter [33]. More recent studies of Glt_{ph} and Glt_{Tk} have dissected the interdependence between substrate and Na^+ binding in detail, concluding that these processes are highly cooperative. Specifically, existing data indicates that two Na^+ ions must bind before the substrate can be recognized [34–36], presumably to sites Na1 and Na3 in the outward-facing conformation. Binding of substrate and of the third ion to the Na2 site would follow. However, this cooperativity is greatly suppressed when Met314 (Met311 in Glt_{ph}) is replaced by Ala or Leu [37], as is the substrate affinity. Although no structures have been reported for any of these mutants, Trp fluorescence measurements show that the pattern of conformational changes in HP2 in response to ion and substrate binding [19, 37] is also subtly altered upon mutation of Met314 [38, 39].

To our knowledge, the precise explanation for these intriguing effects on uptake rates and sodium dependence remains unclear. A plausible hypothesis is that Met314 contributes to defining the Na^+ stoichiometry of the transport reaction; by perturbing the Na2 site, mutation of Met314 would logically slow down the reaction for a given Na^+ concentration gradient, and also partially decouple substrate and Na^+ binding, as observed. Alternatively, it is also plausible that the nature of these effects is primarily kinetic: Met314 might confer a specific order to the occupancy of the substrate and Na2 sites, and contribute to defining their respective affinities, but wild-type and mutant transporters would be, from a thermodynamic and mechanistic standpoint, fundamentally the same. Here we examine the role of Met314 for the Glt_{Tk} transporter through biochemical stoichiometry assays, molecular dynamics simulations, and quantum mechanical calculations.

Materials and Methods

Analysis of the Protein Data Bank

Examples of methionine or cysteine side chains interacting with a sodium ion in known structures were assessed by searching the Protein Data Bank (PDB) as of 2020-10-14. The search was focused on biological assemblies with resolution 3.0 Å or better in which sodium ions are present.

Within that dataset, the distances between the sodium ions and the sulfur atoms of either a Met or Cys side chain were evaluated. A contact was identified when that distance was 3.5 Å or smaller.

Quantum Mechanics (QM) Calculations and NBFIX Corrections

All QM calculations were carried out with Gaussian09 (Gaussian Inc, Wallingford CT, USA). Second-order Møller-Plesset perturbation theory (MP2) with the AUG-cc-pVTZ basis set was used for both geometry optimizations and potential-energy calculations. As analogs of the methionine and cysteine side-chains, we used methylthioethane and methanethiol, respectively. To evaluate the interaction between each analog and a Na^+ ion, the potential energy was calculated for a series of structures in which the distance between the sulfur atom and the ion varies from 2 to 7 Å in 0.1 Å increments. To evaluate the nature of any polarization effects, the charge that is effectively localized in each atom of the analog was evaluated with Natural Bond Orbital (NBO) analysis for three of those structures, at 7.0, 4.0 and 2.8 Å, respectively. The associated electrostatic potentials were then calculated using APBS (www.poissonboltzmann.org) and mapped onto the molecular surface of each analog with PyMol v2.4 (Schrödinger, Inc).

To develop the NBFIX corrections for Met and Cys, analogous sets of 51 configurations were evaluated with NAMD2.9 [40] and the CHARMM36 force field [41, 42], obtaining a potential-energy curve for the default set of Lennard–Jones parameters for each analog. The parameters that specifically describe the S- Na^+ interaction in each case, and R_{min} , were then varied so as to ideally match the MP2 potential energy curves. The range of values scanned for was –5.0 to –14.0 kcal/mol, and 2.7 to 2.8 Å for R_{min} .

Molecular Dynamics (MD) Simulations

All MD simulations were carried out with NAMD2.9 or 2.12 [40] using the CHARMM36 force field [41, 42], supplemented by the NBFIX corrections described above, wherever noted. The simulations were carried out with periodic boundary conditions, constant temperature (298 K), constant semi-isotropic pressure (1 atm), and using an integration time-step of 2 fs. Electrostatic interactions were calculated using the Particle-Mesh Ewald method [43], with a real-space cut-off of 12 Å. Van der Waals interactions were computed with a Lennard–Jones potential, cut off at 12 Å with a smooth switching function taking effect at 10 Å. Analysis was carried out using VMD [44] on snapshots taken every 2 ps.

Simulations of holo- and apo-state Glt_{Tk} in the outward-facing conformation were based on PDB entries 5E9S and 5DWY, respectively [19]. In both cases, the protein was embedded in a pre-equilibrated, hydrated

1-palmitoyl-2-oleoyl-*sn*-glycero-3-phosphocholine (POPC) lipid bilayer using GRIFFIN [45]. Default ionization states were used, and water molecules were added into hydrophilic cavities within the protein using Dowser [46]. The size of the resulting systems is approximately $136 \times 136 \times 87 \text{ \AA}$ and each contains ~ 400 POPC molecules and $\sim 32,000$ water molecules. The simulation systems were equilibrated following a staged protocol comprising a series of restrained simulations. The protocol consists of both positional and conformational restraints, gradually weakened over 150 ns and individually applied to protein side chains and backbone as well as the substrate and Na^+ ions resolved by X-ray crystallography. A trajectory free of any restraints was calculated subsequently. For both the holo state, either with default or NBFIX-corrected CHARMM36, and the apo state, the trajectories calculated are 2 μs long.

An analogous protocol was followed to simulate two variants of the holo-state structure in which the sidechain of Met314 was replaced by Ala or Cys in the three protomers. These trajectories are 500 ns long.

Two additional simulations, each 1 μs long, were carried out in which Na^+ ions were sequentially added to the Na3 and Na1 sites in the wild type apo state. Specifically, we extracted the apo-state configuration observed after 1 μs of MD simulation and added Na^+ ions to the three Na3 sites in the trimer by slowly transforming a nearby water molecule into Na^+ , using the Free Energy Perturbation module in NAMD [40]. In this alchemical transformation, carried out over 50 ns, the appearing sodium ion and the vanishing water molecule were confined to the Na3 site using upper-bound distance restraints. Simultaneously, a Na^+ ion in the solution was transformed into a water molecule, one for each protomer, so as to preserve the net charge of the simulation system. After the transformation was completed, a trajectory of 1 μs was calculated without any restraints. At the end of this trajectory, Na^+ ions were then added to the three Na1 sites in the trimer using the same protocol, and subsequently, a 1 μs -long trajectory was calculated.

Mutagenesis, Expression and Purification

Mutagenesis was carried out using the QuickChange protocol (using primers CAACCATTAATTGCGATGGCACCG CAC and TGCGGTGCCATCGCAATTAATGGTTG for M314C; and CAACCATTAATAGCGATGG CACCGCAC and TGCGGTGCCATCGCTATTAATGGTTG for M314S) on the expression plasmid described in [6]. The constructs were verified by DNA sequencing and transformed in *E. coli* MC1061 cells. Expression and purification were carried out as previously described [47].

Reconstitution into Proteoliposomes

A solution of *E. coli* total lipid extract (20 mg ml^{-1} in 50 mM KPi, pH 7.0) was extruded with a 400-nm-diameter polycarbonate filter (Avestin, 11 passages) and diluted with the same buffer to a final concentration of 5 mg ml^{-1} . The lipid mixture was destabilized with 10% Triton-X100. Purified Glt_{Tk} and the destabilized lipids were mixed in a ratio of 1:250 (protein: lipid) and incubated at room temperature for 30 min. Bio-beads were added four times (25 mg ml^{-1} , 15 mg ml^{-1} , 19 mg ml^{-1} , 29 mg ml^{-1} lipid solution) after 0.5 h, 1 h, overnight and 2 h incubation, respectively, on a rocking platform at 4 °C. The Bio-beads were removed by passage over an empty Poly-Prep column (Bio-Rad). The proteoliposomes were collected by centrifugation (20 min, 298,906 g, 4 °C), subsequently resuspended in 50 mM KPi, pH 7.0 to the lipid concentration of 20 mg ml^{-1} and freeze-thawed for three cycles. The proteoliposomes were stored in liquid nitrogen until subsequent experiments.

Measuring Transporter Equilibrium Potentials

Stored proteoliposomes were thawed and collected by centrifugation (20 min, 298,906 g, 4 °C), the supernatant was discarded and the proteoliposomes were resuspended to a concentration of 10 mg ml^{-1} of lipids in buffer containing 20 mM Hepes/Tris, pH 7.5, 200 mM NaCl, 50 mM KCl, 10 μM L-aspartate (containing 1 μM [^3H]-L-aspartate). The internal buffer was exchanged by three cycles of freezing in liquid nitrogen and thawing, and finally extruded through a polycarbonate filter with 400 nm pore size (Avestin, 11 passages). The experiment was started by diluting the proteoliposomes 20 times into a buffer containing 20 mM Hepes/Tris, pH 7.5, 200 mM NaCl, 3 μM valinomycin, and varying concentrations of KCl and Choline Cl were added in order to obtain the membrane potentials -78.06 mV , -39.03 mV and -26.02 mV , which are the calculated reversal potentials for hypothetical 4:1, 3:1 and 2:1 $\text{Na}^+:\text{L-asp}$ stoichiometries (35.0/26.4/19.2 mM CholineCl, 0/11.1/18.4 mM KCl).

After 1, 2 and 3 min the reaction was quenched with ice-cold quenching buffer containing 20 mM Hepes/Tris, pH 7.5, 250 mM Choline Cl and immediately filtered on nitrocellulose filter (Protran BA 85-Whatman filter). Finally, the filter was washed with 2 ml of quenching buffer. The flux of radiolabeled aspartate was measured by subtracting the amount of radiolabeled aspartate at 1 min from the amount of radiolabeled substrate at 3 min. The filters were dissolved in scintillation cocktail and the radioactivity was measured with a PerkinElmer Tri-Carb 2800RT liquid scintillation counter. The equilibrium, or reversal, potential, E_{rev} , for each condition was calculated as described in [48].

Results and Discussion

Polarization Effects Explain Atypical Methionine Coordination of Na⁺

As mentioned above, the observation that the methionine in the conserved NMDGT motif coordinates the Na⁺ ion in the Na2 site is, statistically speaking, highly atypical, given its hydrophobic character [49]. However, close-range contacts between methionines and the guanidinium and amino groups in arginines and lysines are common in known protein structures [50], as are interactions with carboxyl and carbonyl groups [51], and aromatic rings [51, 52]. This striking promiscuity indicates the sulfur atom in the methionine side chain is highly polarizable, i.e., it can alter its electrostatic character to better match its near environment. To examine whether this polarizability might also explain the interaction observed in the Na2 site in SLC1-family Na⁺-dependent transporters, we carried out a series of MP2-level quantum-mechanical calculations in which a Na⁺ ion was gradually brought closer to the sulfur atom in the methionine side chain analog methylthioethane, and evaluated the resulting interaction energy as well as the change in their electronic charge distribution. As shown in Fig. 2a (blue curve), this interaction is unequivocally attractive, favoring a contact distance between ion and sulfur of about 2.8 Å, which closely resembles what is observed in the structure of Glt_{TK}, namely 3.0 Å (on average). Further examination of these results with Natural Bond Orbital calculations reveals how the distribution of atomic charges in the analog is gradually altered as the Na⁺ ion becomes closer, with the sulfur becoming significantly more electronegative, and its flanking groups more electropositive (Fig. 2b).

To examine this interaction in the context of the structure of the transporter, we turned to all-atom molecular dynamics (MD) simulations. Specifically, we designed a simulation system including a wild-type Glt_{TK} trimer in the outward-occluded conformation, with three Na⁺ ions and one L-Asp molecule bound in each protomer, embedded in a model phospholipid bilayer and a 100 mM NaCl solution; the resulting system thus comprises over 170,000 atoms (Fig. S1). To be able to calculate trajectories probing the microsecond timescale for such a system, and thus derive statistically significant data, we used a fixed-charged energy function, namely the CHARMM36 force field. A caveat of this and comparable force fields, however, is that they do not include electronic polarizability effects such as those discussed above. The CHARMM36 representation of methionine, for example, is adequate for a hydrophobic entity, but as shown in Fig. 2a (red curve), it fails to capture the emergence of an attractive interaction

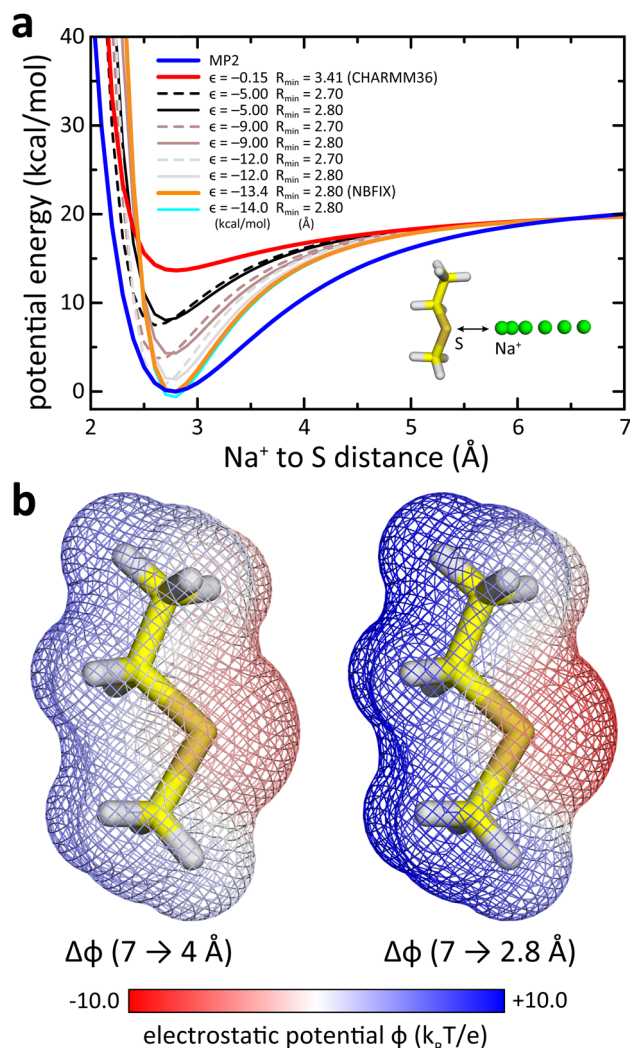


Fig. 2 Polarization of the methionine side chain by close proximity with a sodium ion. **a** Change in the potential energy of a system comprising a methionine analog and a Na⁺ ion (inset) as the distance between the ion and the sulfur atom is varied from 7 to 2 Å. Quantum mechanical calculations at the MP2 level (thick blue line) are compared with values calculated with the standard CHARMM36 molecular-mechanics force field (thick red line), as well as with a series of modifications thereof in which the Lennard–Jones parameters used for the S–Na⁺ interaction are varied. Results are shown for values ranging from -5.0 to -14.0 kcal/mol and for R_{\min} values from 2.7 Å (dashed lines) to 2.8 Å (solid lines). The values of the NBFIX correction implemented in this study are $\epsilon = -13.4$ kcal/mol and $R_{\min} = 2.8$ Å (thick orange line). **b** Change in the electrostatic potential that results from the change in the methionine analog atomic charges when the Na⁺ ion approaches the sulfur atom from 7 to 4 Å (left), or from 7 to 2.8 Å (right), i.e., the potential-energy minimum. The potential is mapped onto the surface of the analog (mesh). Larger contrast between positive (blue) and negative (red) values indicates a higher degree of polarization by Na⁺

between Na⁺ and the sulfur atom, precisely because the atomic charges are constant. Accordingly, an MD trajectory of our holo-state Glt_{TK} trimer using this force field showed irreversible dissociation of the Na⁺ ion at the

Na2 site, in all three protomers, within 500 ns of simulation time (Fig. 3a). Further analysis shows this instability specifically results from a defective representation of the interaction with Met314, which breaks off immediately after the ion and side chain atoms are allowed to move freely (Fig. 3a). This observation is consistent with the conclusions of an independent simulation study of Glt_{TK}, reported while this study was underway [53]. Indeed, irreversible dissociation of the Na2 ion appears to have been a common denominator of simulation studies of the mechanisms of both Glt_{Ph} and Glt_{TK} [19, 54–56]. It is however straightforward to recognize this observation is artefactual. The dissociation constant of the Na2 site, while L-Asp is

bound, has been estimated to be 10–100 μM [57], which is 3–4 orders of magnitude smaller than the concentration of free Na⁺ in simulation systems ($\sim 100 \text{ mM}$). The corresponding off-rate was also estimated at 100 per second [57]. It is clear, therefore, that irreversible dissociation of the ion in Na2 in microsecond scale simulations reflects a systematic methodological problem, rather than a mechanistically significant event.

A convenient approach to correct this type of force field deficiency, used previously for other problematic ion-protein interactions in CHARMM36 [58–61], is to customize the generic Lennard–Jones (LJ) potential by introducing parameters specifically designed to improve the interaction

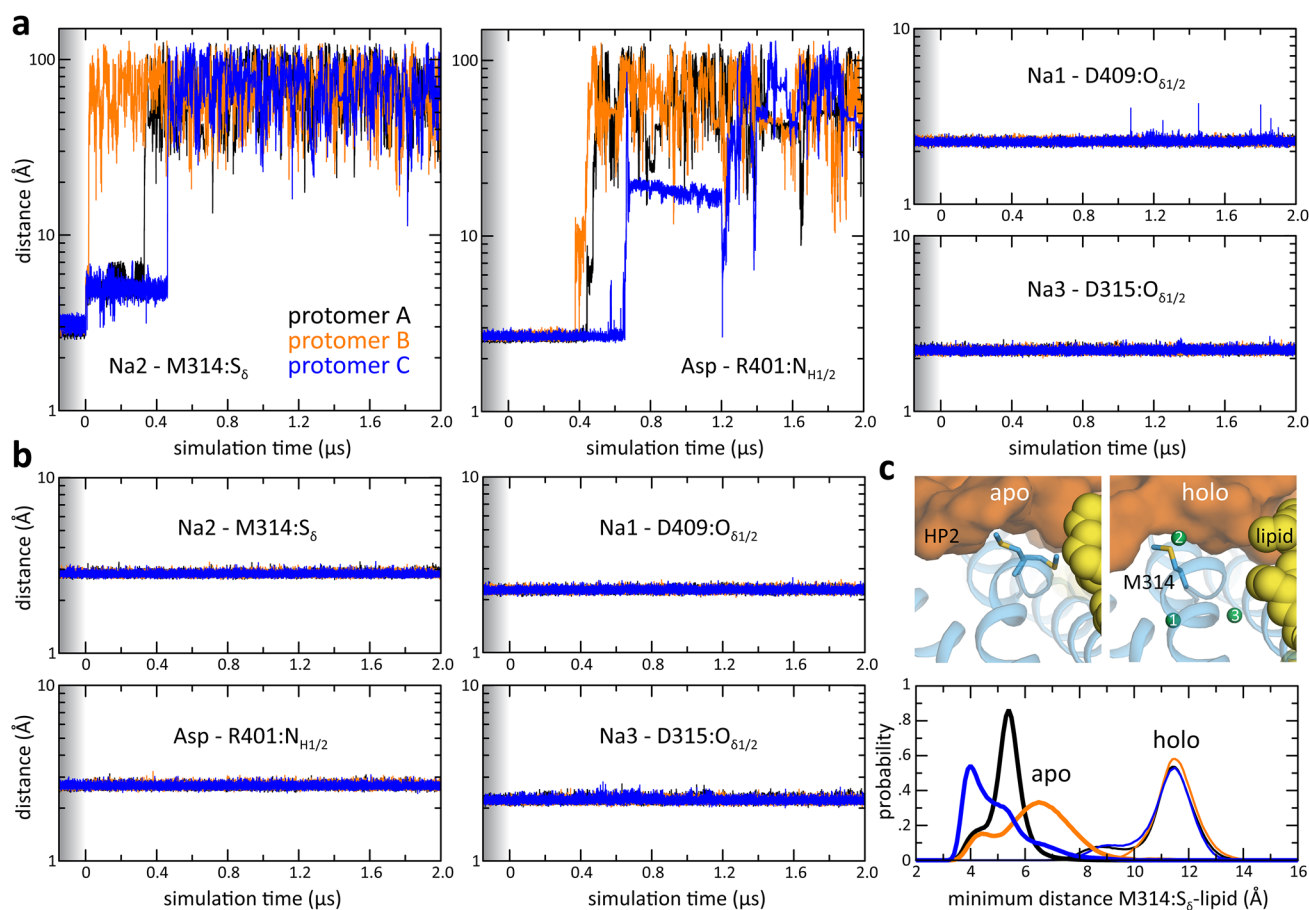


Fig. 3 MD simulations of wild type holo-state Glt_{TK} trimer with standard and corrected force fields. **a** Using standard CHARMM36, the Na⁺ ions at the Na2 sites rapidly unbind, followed by L-aspartate. The dissociation of the Na⁺ ion from Na2 (*left*) is measured by its distance to the sulfur atom in Met314, for each of the three protomers (*black, orange and blue lines*) and as a function of simulation time. The dissociation of L-aspartate was measured relative to the nearest terminal N atom of Arg401 (*center*). Ions at Na1 and Na3 are, in contrast, stably bound, as measured by the distance, respectively, to the Asp409 and Asp315 sidechain terminal O atoms (*right*). In all plots, the shaded area prior to $t=0$ ns indicates the progressive reduction of conformational and distance restraints acting on the complex

during the equilibration stages. **b** Using the NBFIX correction of Na⁺-methionine interactions, all Na⁺ ions and the substrate remain stably bound throughout the trajectory. **c** Orientation of the Met314 side chain toward the hydrophobic lipid bilayer is preserved in simulations of the apo transporter that also use the NBFIX correction. Upper: simulation snapshots are shown with the protein as cartoon helices, the sidechain of Met314 in sticks, HP2 as an orange surface and nearby lipid tails in yellow spheres. Lower: Distribution of distances between the sulfur atom and the nearest lipid tail atom in simulations of the apo (*thick lines*) and fully-occupied (holo, *thin lines*) transporter, with individual lines indicating different protomers in the same trajectory

in question. As shown in Fig. 2a (orange curve) for the Na^+ -methionine interaction, optimized LJ parameters for S and Na^+ indeed result in a very reasonable agreement between quantum–mechanical data and the now-corrected CHARMM36, particularly at close range. Reassuringly, a simulation of the holo-state Glt_{TK} trimer carried out using this so-called NBFIX correction showed stable occupancy of the Na2 site (Fig. 3b), similar to the ions in the Na1 and Na3 binding sites (Fig. 3a, b). The presence of the ion at the Na2 site also stabilizes the L-aspartate in its binding site (Fig. 3b), unlike in the simulations without the force field correction, where the L-aspartate substrate dissociated subsequent to the Na2 ion (Fig. 3a). Stable binding of substrate and ions is arguably the expected outcome for microsecond-long simulations of this occluded-state wild-type transporter. It is important to note that this NBFIX correction does not impact any other interactions involving a methionine (or a Na^+ ion), unlike what results from modification of the atomic charges [53]. Thus, all methionine residues in the simulation system, and Met314 in particular, preserve their primary character, which is hydrophobic. This factor is key because, in the apo-state of Glt_{TK} and Glt_{ph} , Met314 reorients away from the Na2 site and becomes surrounded by other hydrophobic side chains [6, 37]. Owing to the specificity of the NBFIX correction, this intriguing duality is recapitulated in our simulations (Fig. 3c); indeed, the data shows that in apo Glt_{TK} , Met314 is also exposed to the hydrocarbon interior of the lipid bilayer.

Met314 Does Not Define the Na^+ Stoichiometry of Glt_{TK}

As mentioned, experimental mutation of the methionine in the NMDGT motif has clear effects on the function of both EAAT2/3 [21, 23, 33] and Glt_{ph} [37–39]. Some of these observations, taken together with the nature of the Na^+ -methionine interaction discussed above, could be interpreted as evidence that this methionine is essential for defining the 3:1 stoichiometry of the coupled ion-substrate transport reaction. To examine this hypothesis experimentally, we determined the ion-substrate stoichiometry in wild-type Glt_{TK} or in mutants in which Met314 was replaced by cysteine, serine, alanine or leucine, using purified protein reconstituted in proteoliposomes. To do so, we quantified the extent of Na^+ -coupled L-aspartate influx or efflux in conditions that would strongly favor efflux (a 20-fold outward gradient in L-Asp), were it not for an outward transmembrane electrical potential, experimentally generated as a potassium diffusion potential using the ionophore valinomycin (Fig. 4a inset). Because co-transport of Na^+ and L-Asp moves positive charge across the membrane, this outward potential not only opposes L-Asp efflux, but can also drive uphill influx at sufficiently large (negative) values. The value at which no

net flux occurs, referred to as the reversal potential, depends on the number of Na^+ ions co-transported with L-Asp, and can be estimated a priori [48, 62, 63]. Here, we examined the effect of K^+ diffusion potentials that would result in a zero-flux equilibrium in hypothetical reactions requiring 4, 3 or 2 Na^+ ions in our specific experimental conditions. The results for WT Glt_{TK} showed that this ‘reversal potential’ is -39 mV, which corresponds to a 3:1 stoichiometry (Fig. 4a). As expected, the smaller (less negative) potential allows for downhill efflux of L-Asp while the larger (more negative) potential has the opposite effect, and drives L-Asp into the liposomes, uphill. This result reproduces our previous measurements [15, 47] and is satisfyingly consistent with the structural data [19]. Surprisingly, however, analogous experiments for M314C and M314S demonstrate that the stoichiometry of the transport reaction is also 3:1 (Fig. 4b, c). M314A was only marginally stable in detergent solution and thus difficult to characterize conclusively, but the trends in the data suggest that its stoichiometry is also unchanged relative to WT (Fig. 4d). Unfortunately, M314L could not be characterized due to low expression levels.

It is not self-evident how to rationalize these observations at the structural level. While serine side chains are often observed in Na^+ binding sites coordinating the ion via their hydroxyl oxygen, cysteine and alanine side chains are uncommon [64]. Thus, to clarify these experimental results, we again turned to computer simulations. Specifically, for both M314A and M314C, we calculated MD trajectories analogous to those discussed above for the holo WT Glt_{TK} trimer, i.e., with three Na^+ ions and one L-Asp molecule initially bound to each protomer. (The S- Na^+ interaction in the cysteine mutant was corrected following the same procedure as for methionine (Fig. S2a)). Consistent with the stoichiometry measurements, the Na^+ ion at the Na2 site remained bound throughout these trajectories (Fig. 5b, c). In M314A, we observed that water coordinated the ion, along with the side-chain hydroxyl of Thr355, and thereby compensated for the lack of the thioether group in the wild-type structure, allowing the position of the ion to remain largely unchanged (Fig. 5a, b, d, e). In M314C, water molecules were also seen to participate in the coordination of the ion, as did the sulfur atom in the cysteine side chain (Fig. 5c, f), owing to polarizability effects comparable to those observed for methionine (Fig. S2b).

Taken together, measurements and simulations of WT and mutant Glt_{TK} demonstrate that the Met314 sidechain is not required for occupation of Na2 by Na^+ , despite its role in ion coordination in the WT transporter. It seems reasonable to conclude, therefore, that the thermodynamics of the transport mechanism of Glt_{TK} , and by extension other Na^+ -coupled transporters in this family, is not fundamentally defined by the conserved methionine in the NMDGT motif through its contribution to the Na2 site. While this

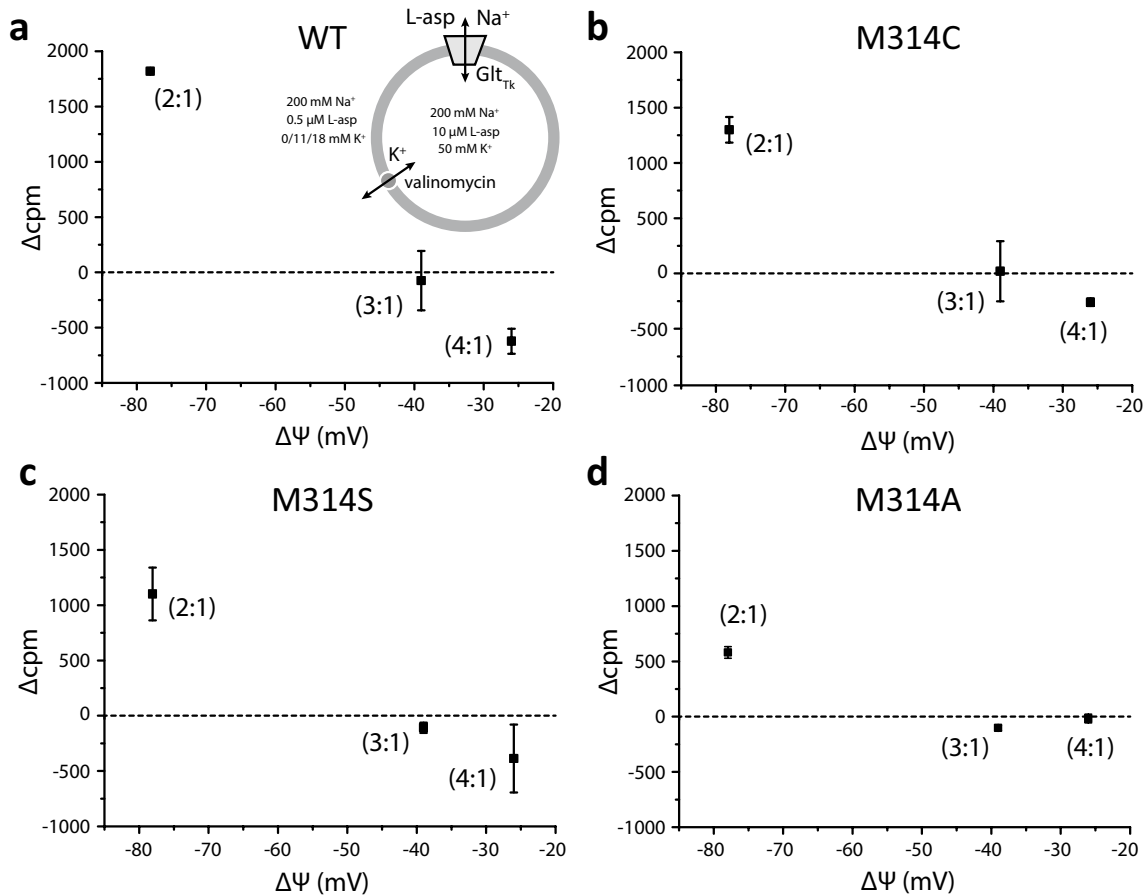


Fig. 4 Determination of Na⁺:aspartate coupling stoichiometry using equilibrium potential measurements. Inset: Schematic of the experimental protocol used for proteoliposomes containing (a) wild type Glt_{Tk} protein and Met314 mutants (b) M314C, (c) M314S, and (d) M314A. The uptake or efflux of radiolabeled aspartate was determined by comparing the luminal radioactivity associated with the

liposomes after 3 min of incubation with the radioactivity present after 1 min (Δ cpm). For each membrane voltage probed, numbers in parentheses indicate the coupling stoichiometry that would be consistent with a zero-flux condition, if this condition had been observed. Error bars represent the \pm SD obtained from 2 replicates

residue causes substrate and Na⁺ binding to be cooperative, this cooperativity is not essential for enforcing the stoichiometry of the transport cycle, implying that other factors more fundamentally control the coupling mechanism of this transporter.

HP2 Occlusion as a Rationale for Stoichiometric Coupling

Previous studies of the Na⁺/Ca²⁺ exchanger NCX_{Mj}, also a secondary-active transporter, might provide clues into the nature of those factors. NCX_{Mj} translocates either 3 Na⁺ or 1 Ca²⁺ across the membrane [63], and thus functions as an antiporter. A systematic examination of the conformational energy landscape of NCX_{Mj}, using molecular simulations and X-ray crystallography, concluded that the interconversion between open and occluded states is the process that explains the stoichiometry of the transport cycle, i.e., the

origin of the coupling mechanism [59]. Specifically, the authors found that occluded conformations, which are necessary intermediates in the alternating-access transition, are energetically accessible only when 3 Na⁺ or 1 Ca²⁺ are bound [59], partial or no ion occupancies, or H⁺ binding to the Na⁺/Ca²⁺ sites, do not permit occlusion, and accordingly do not catalyze transport. Consistent with this view, a recent study of Glt_{ph} and a crystallizable EAAT1 variant suggests that the observation of K⁺ antiport correlates with the feasibility of HP2 closure after K⁺ binding [65].

Our simulations of Glt_{Tk} provide support that this notion will apply to the substrate-Na⁺ stoichiometry in Glt_{Tk} as well. As noted above, in trajectories using conventional CHARMM36, we observe ready dissociation of Na⁺ from Na2 followed by L-aspartate (Fig. 3a). The order and time-scale of these events is, as discussed, artefactual, but the resulting configuration, only occupied by Na⁺ in Na1 and Na3, is a mechanistically relevant state in physiological

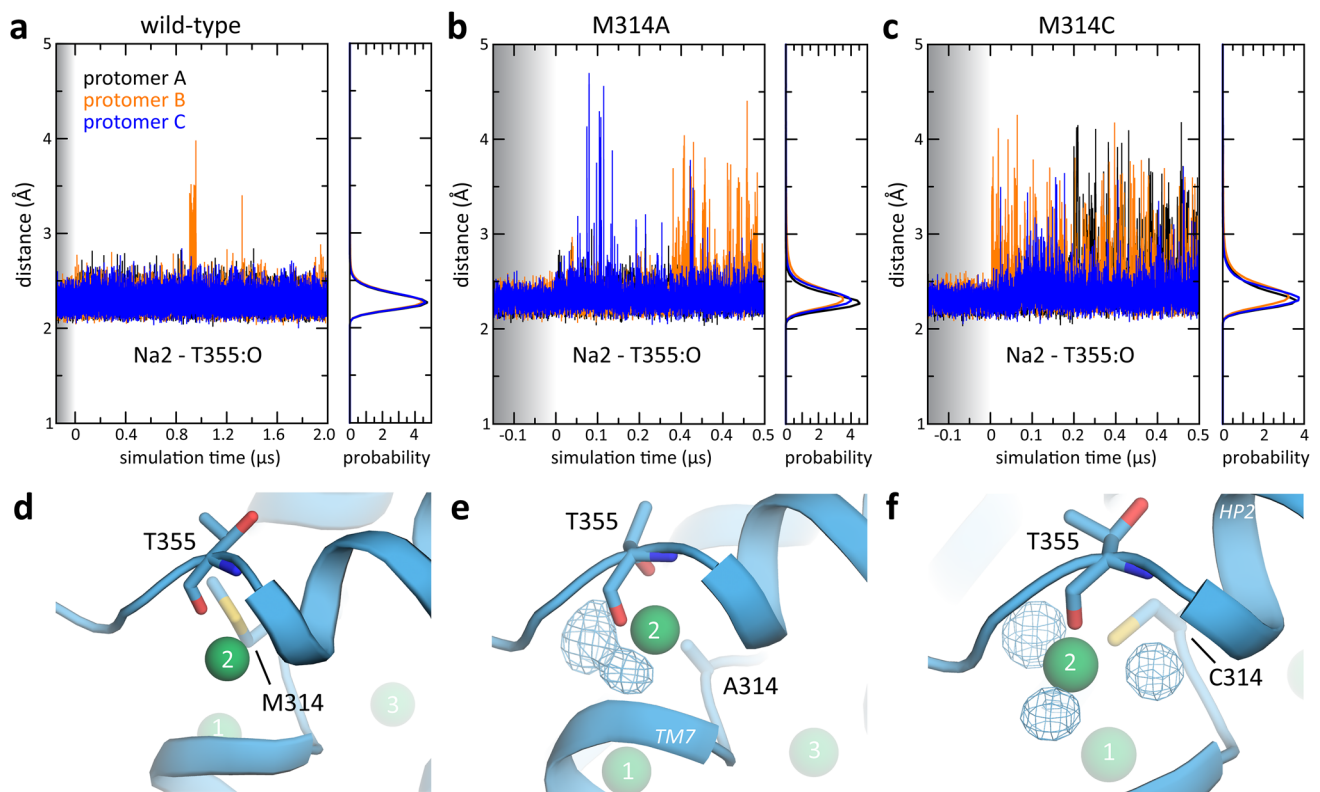
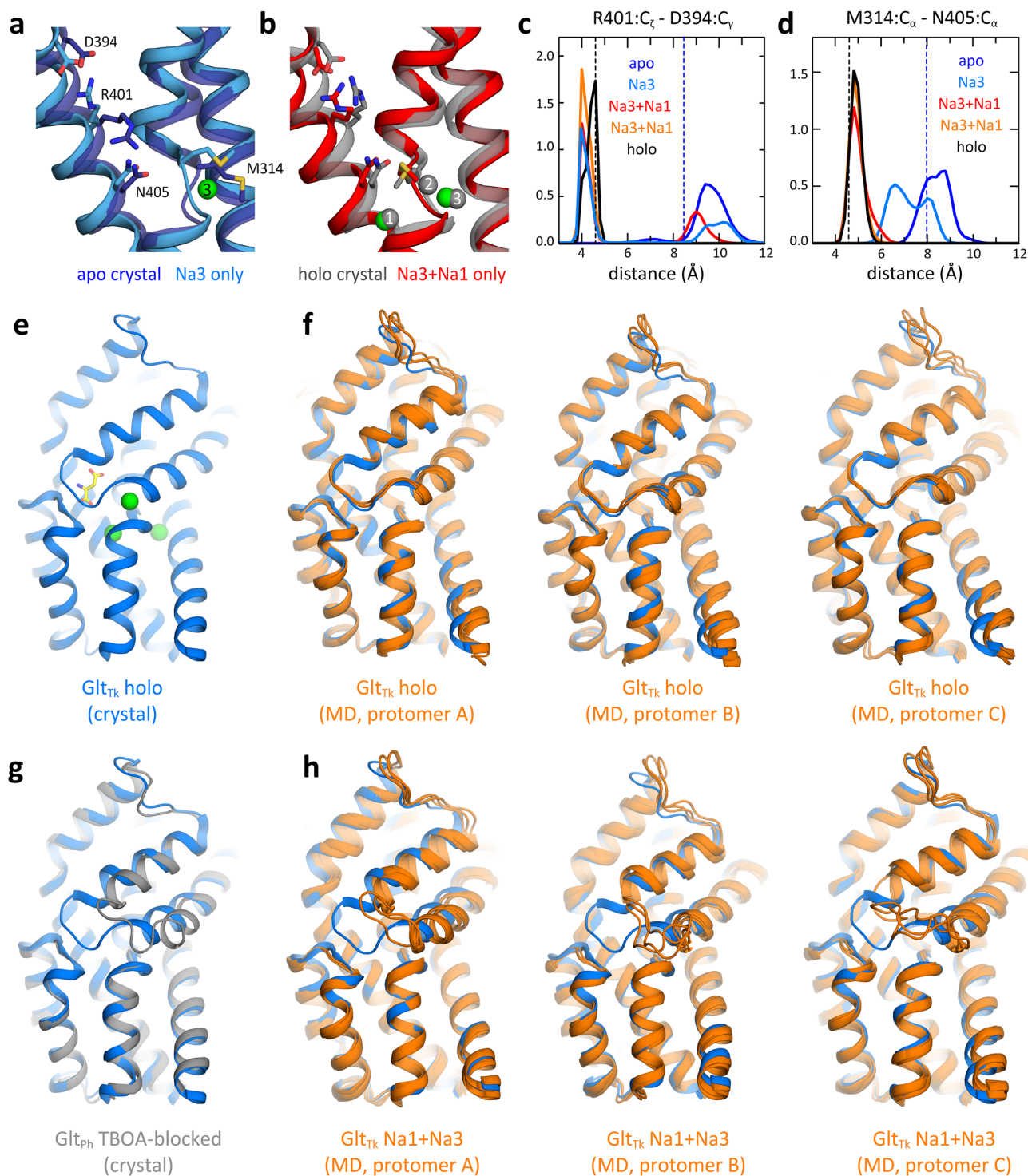


Fig. 5 Ion and water occupancy in Glt_{Tk} mutants during MD simulations. **a–c** The coordination of the sodium ion in Na2 by the backbone carbonyl of Thr355 is monitored by the Na⁺-O distance, shown as a function of time (*left panel*) and as a distribution over time (*right panel*) for each of the three protomers in the simulation (*black, orange, blue*) for wild-type (**a**), M314A (**b**), and (**c**) M314C. **d–f** Close-up of Na2 binding sites in representative snapshots of the sim-

ulations of wild-type (**a**), M314A (**b**), and (**c**) M314C, indicating the location of the sodium ions (*green spheres*). Water molecules found to be involved in Na⁺ coordination in M314A and M314C are represented by density signals (*blue mesh*), directly calculated from the MD trajectories and averaged over the three protomers in the trimer. The protein backbone is shown as cartoon helices, and key side chains are shown as sticks

conditions [34–36]. In agreement with recently-published structures of inward-facing Glt_{Tk} [10] and outward-facing Glt_{ph} [38], we observe that this outward-facing, partially-occupied state preserves many of the key features of the holo-state structure [19]. For example, the ion-pair between Arg401 and Asp394, which primes Arg401 for substrate coordination (Figs. 1b and 6a, c), is present. In addition, the configuration of Met314 in this state permits Na⁺ coordination at the Na2 site (Fig. 6b, d). Independent simulations initiated in the apo state, where Na⁺ ions were sequentially added at the Na3 and Na1 sites, corroborate these findings. These trajectories show that occupancy of Na3 alone controls the conformation of Arg401 (Fig. 6a, c), seemingly through their electrostatic repulsion. However, binding at Na3 alone is not sufficient to reorganize the backbone or side chain of Met314, even though Asn313 and Asp315, which flank Met314, both contribute side chains to the Na3 site. Only when Na1 is also occupied does Met314 reorient to match the geometry conducive to ion binding at the Na2 site (Fig. 6b, d).

This partially occupied state, however, lacks a central feature of the holo-state structure, namely HP2 in a configuration that occludes the binding sites (Fig. 6e). Invariably, the absence of L-Asp and the third ion at the Na2 site leads to the opening of this hairpin towards the extracellular space, which after 1 μs of simulation adopts a conformation closely resembling that observed in structures of Glt_{ph} and Glt_{Tk} bound to blockers [5, 10] (Fig. 6g, h), and in a recently-reported structure of Glt_{ph} in the same partially occupied state [38]. By contrast, extended simulations of the fully-occupied transporter (made possible by the NBFIX correction described above) demonstrate that the presence of all ions and the substrate correlates with HP2 favoring the occluded conformation (Fig. 6f). These results indicate that the energy landscape governing the dynamics of HP2, and by extension the occlusion of the transporter and the viability of the alternating-access transition, is indeed re-shaped by the occupancy or vacancy of the ion and substrate binding sites. In other words, opening of HP2 does appear to serve as the



structural mechanism that prevents uncoupled transport, as suggested elsewhere [37, 38]. Further experimental and computational investigations will be required to continue to examine this hypothesis and fully clarify its molecular basis.

Conclusions

Most secondary-active transporters couple the uptake or efflux of substrates to the co-translocation of ions in well-defined stoichiometries. This coupling is the defining

Fig. 6 Conformation of Glt_{TK} in a partially occupied state with Na^+ ions at Na3 and Na1. **a** The crystal structure of the apo-state transporter (PDB entry 5E9S, *dark blue*) is superposed on a snapshot of the simulation of the apo state in which a single sodium ion (*green sphere*) was added to the Na3 site (*light blue*), with key side chains shown as sticks and labelled. **b** The crystal structure of the fully-occupied transporter (PDB entry 5DWY, *gray*) is superposed on a snapshot of the simulation in which two sodium ions were sequentially added at the Na3 and Na1 sites (*red*). **c** Distance between the side chain terminal carbon atoms of Arg401 and Asp394, shown as a probability histogram over time, for simulations of fully-occupied Glt_{TK} (*black, holo*); the apo state (*blue*); a hypothetical intermediate occupied only at the Na3 site (*light blue*); and a state occupied at the Na3 and Na1 sites, either after release of Na2 and L-Asp (*orange*) or after addition of ions to the apo state (*red*). The formation of a salt-bridge between Arg401 and Asp394 primes the former to coordinate the substrate and requires binding of Na^+ to Na3. The values of this distance in the crystal structures of apo (*blue*) and holo (*black*) transporter are shown as dashed vertical lines. **d** Distance between the C α atoms of Met314 and Asn405 in TM8, shown as in **(c)**. Binding of Na^+ to Na1, with Na3 already occupied, recruits backbone atoms adjacent to Met314, and positions its sidechain for coordination of the third ion, at the Na2 site. **e** Crystal structure of the outward-facing holo-state of Glt_{TK} , highlighting the configuration of HP2 that occludes access to the Na^+ and substrate binding sites. **f** HP2 remains closed during simulations of the holo-state transporter, as observed in the holo-state crystal structure (*blue*). Simulation snapshots (*orange*) are shown for each of the three protomers, taken at 1.0, 1.5 and 2.0 μs . **g** The crystal structure of the occluded holo-state of Glt_{TK} (*blue*) is compared with the crystal structure of TBOA-bound Glt_{Ph} (*gray*) (PDB entry 2NWW). **h** HP2 opens during simulations in which only Na1 and Na3 are occupied, adopting a conformation comparable to that observed in the crystal structure of TBOA-bound Glt_{Ph} . Simulation snapshots are shown (*orange*) for each of the three protomers, taken at 1.0, 1.5 and 2.0 μs , and superposed on the crystal structure of holo Glt_{TK} (*blue*)

functional feature of this class of proteins, as it permits them to harness transmembrane electrochemical gradients, usually of Na^+ or H^+ , to power substrate transport, even against an opposing concentration gradient. The general principles that explain this coupling, however, remain to be clearly established. In Na^+ -dependent transporters of the SLC1 family, substrate and Na^+ binding are strongly cooperative; therefore, it is intuitive to infer that this cooperativity in binding is what explains the substrate-ion coupling of the transport reaction. However, mutation of a conserved methionine in the so-called NMDGT motif greatly impairs this cooperativity in binding, and while it also slows down the turnover rate, our data shows that it does not impact the stoichiometry of the transport cycle. Therefore, we conclude that while cooperativity in binding can be a form of kinetic optimization, the stoichiometric coupling of substrate and ion transport is more fundamentally explained by other factors. A structural mechanism whereby only selected occupancy states permit the transporter to adopt occluded conformations, as it transitions between outward and inward-open states, is a likely explanation.

Supplementary Information The online version of this article (<https://doi.org/10.1007/s11064-021-03253-w>) contains supplementary material, which is available to authorized users.

Acknowledgements This research was funded by the Divisions of Intramural Research of the National Institute of Neurological Disorders and Stroke (LRF) and of the National Heart, Lung and Blood Institute (WZ and JDFG), National Institutes of Health (NIH), USA; and by the Nederlandse Organisatie voor Wetenschappelijk Onderzoek 714.018.003 and 711.017.012 (GT and DJS). Computational resources were provided, in part, by the NIH HPC facility Biowulf.

Open Access This article is licensed under a Creative Commons Attribution 4.0 International License, which permits use, sharing, adaptation, distribution and reproduction in any medium or format, as long as you give appropriate credit to the original author(s) and the source, provide a link to the Creative Commons licence, and indicate if changes were made. The images or other third party material in this article are included in the article's Creative Commons licence, unless indicated otherwise in a credit line to the material. If material is not included in the article's Creative Commons licence and your intended use is not permitted by statutory regulation or exceeds the permitted use, you will need to obtain permission directly from the copyright holder. To view a copy of this licence, visit <http://creativecommons.org/licenses/by/4.0/>.

References

1. Grewer C, Gameiro A, Rauen T (2014) SLC1 glutamate transporters. *Pflügers Archiv - Eur J Physiol* 466(1):3–24
2. Vandenberg RJ, Ryan RM (2013) Mechanisms of glutamate transport. *Physiol Rev* 93(4):1621–1657
3. Amara SG (1992) A tale of two families. *Nature* 360(6403):420–421
4. Kanner Baruch I 1997 Sodium-Coupled GABA and Glutamate Transporters.” In: Maarten E. A. Reith (Ed) Neurotransmitter Transporters: Structure, Function, and Regulation, Totowa, NJ: Humana Press, pp. 151–69.
5. Boudker O, Ryan RM, Yernool D, Shimamoto K, Gouxau E (2007) Coupling substrate and ion binding to extracellular gate of a sodium-dependent aspartate transporter. *Nature* 445(7126):387–393
6. Jensen S, Guskov A, Rempel S, Hänel I, Slotboom DJ (2013) Crystal structure of a substrate-free aspartate transporter. *Nat Struct Mol Biol* 20(10):1224–1226
7. Yernool D, Boudker O, Jin Y, Gouxau E (2004) Structure of a glutamate transporter homologue from *Pyrococcus horikoshii*. *Nature* 431(7010):811–818
8. Canul-Tec JC, Assal R, Cirri E, Legrand P, Brier S, Chamot-Rooke J, Reyes N (2017) Structure and allosteric inhibition of excitatory amino acid transporter 1. *Nature* 544:446–451
9. Groeneveld M, Slotboom DJ (2007) Rigidity of the subunit interfaces of the trimeric glutamate transporter GltT during translocation. *J Mol Biol* 372(3):565–570
10. Arkhipova V, Guskov A, Slotboom DJ (2020) Structural ensemble of a glutamate transporter homologue in lipid nanodisc environment. *Nat Commun* 11(1):998
11. Crisman TJ, Shaogang Qu, Kanner BI, Forrest LR (2009) Inward-facing conformation of glutamate transporters as revealed by their inverted-topology structural repeats. *Proc Natl Acad Sci USA* 106(49):20752–20757
12. Garaeva AA, Slotboom DJ (2020) Elevator-type mechanisms of membrane transport. *Biochem Soc Trans* 48(3):1227–1241

13. Reyes N, Ginter C, Boudker O (2009) Transport mechanism of a bacterial homologue of glutamate transporters. *Nature* 462(7275):880–885
14. Zhou W, Fiorin G, Anselmi C, Karimi-Varzaneh HA, Poblete H, Forrest LR, Faraldo-Gómez JD (2019) Large-scale state-dependent membrane remodeling by a transporter protein. *eLife* 8:e50576
15. Groeneveld M, Slotboom DJ (2010) Na(+):aspartate coupling stoichiometry in the glutamate transporter homologue Glt(Ph). *Biochemistry* 49(17):3511–3513
16. Levy LM, Warr O, Attwell D (1998) Stoichiometry of the glial glutamate transporter GLT-1 expressed inducibly in a chinese hamster ovary cell line selected for low endogenous Na⁺-dependent glutamate uptake. *J Neurosci* 18(23):9620–9628
17. Owe SG, Marcaggi P, Attwell D (2006) The ionic stoichiometry of the GLAST glutamate transporter in salamander retinal glia. *J Physiol* 577(Pt 2):591–599
18. Zerangue N, Kavanaugh MP (1996) Flux coupling in a neuronal glutamate transporter. *Nature* 383(6601):634–637
19. Guskov A, Jensen S, Faustino I, Marrink SJ, Slotboom DJ (2016) Coupled binding mechanism of three sodium ions and aspartate in the glutamate transporter homologue Glt_{TK}. *Nature Communications* 7(1):13420
20. Ryan RM, Compton ELR, Mindell JA (2009) Functional characterization of a Na⁺-dependent aspartate transporter from *Pyrococcus horikoshii*. *J Biol Chem* 284(26):17540–17548
21. Borre L, Kanner BI (2001) Coupled, but not uncoupled, fluxes in a neuronal glutamate transporter can be activated by lithium ions. *J Biol Chem* 276(44):40396–40401
22. Tao Z, Zhang Z, Grever C (2006) Neutralization of the aspartic acid residue Asp-367, but Not Asp-454, inhibits binding of Na⁺ to the glutamate-free form and cycling of the glutamate transporter EAAC1. *J Biol Chem* 281(15):10263–10272
23. Zarbiv R, Grunewald M, Kavanaugh MP, Kanner BI (1998) Cysteine scanning of the surroundings of an alkali-ion binding site of the glutamate transporter GLT-1 reveals a conformationally sensitive residue. *J Biol Chem* 273(23):14231–14237
24. Zhang Y, Bendahan A, Zarbiv R, Kavanaugh MP, Kanner BI (1998) Molecular determinant of ion selectivity of a (Na⁺ + K⁺)-coupled rat brain glutamate transporter. *Proc Natl Acad Sci USA* 95(2):751–755
25. Coleman JA, Green EM, Gouaux E (2016) X-ray structures and mechanism of the human serotonin transporter. *Nature* 532(7599):334–339
26. Ficici E, Zhou W, Castellano S, Faraldo-Gómez JD (2018) Broadly conserved Na⁺-binding site in the N-lobe of prokaryotic multidrug MATE transporters. *Proc Natl Acad Sci USA* 115(27):E6172–E6181
27. Lee C, Kang HJ, von Ballmoos C, Newstead S, Uzdavins P, Dotson DL, Iwata S, Beckstein O, Cameron AD, Drew D (2013) A two-domain elevator mechanism for sodium/proton antiport. *Nature* 501(7468):573–577
28. Marinelli F, Almagor L, Hiller R, Giladi M, Khananshvil D, Faraldo-Gómez JD (2014) Sodium recognition by the Na⁺/Ca²⁺ exchanger in the outward-facing conformation. *Proc Natl Acad Sci USA* 111(50):E5354–E5362
29. Meier T, Krah A, Bond PJ, Pogoryelov D, Diederichs K, Faraldo-Gómez JD (2009) Complete ion-coordination structure in the rotor ring of Na⁺-dependent F-ATP synthases. *J Mol Biol* 391(2):498–507
30. Berman HM, Westbrook J, Feng Z, Gilliland G, Bhat TN, Weissig H, Shindyalov IN, Bourne PE (2000) The Protein Data Bank. *Nucleic Acids Res* 28(1):235–242
31. Raunser S, Appel M, Ganea C, Geldmacher-Kaufner U, Fendler K, Kühlbrandt W (2006) Structure and function of prokaryotic glutamate transporters from *Escherichia coli* and *Pyrococcus horikoshii*. *Biochemistry* 45(42):12796–12805
32. Groeneveld M, Detert Oude Weme RGJ, Durkens RH, Slotboom DJ (2010) Biochemical characterization of the C4-dicarboxylate transporter DctA from *Bacillus subtilis*. *J Bacteriol* 192(11):2900–2907
33. Rosental N, Kanner BI (2010) A conserved methionine residue controls the substrate selectivity of a neuronal glutamate transporter. *J Biol Chem* 285(28):21241–21248
34. Ewers D, Becher T, Machtens J-P, Weyand I, Fahlke C (2013) Induced fit substrate binding to an archeal glutamate transporter homologue. *Proc Natl Acad Sci USA* 110(30):12486–12491
35. Reyes N, Oh SC, Boudker O (2013) Binding thermodynamics of a glutamate transporter homolog. *Nat Struct Mol Biol* 20(5):634–640
36. Hänelt I, Jensen S, Wunnicke D, Slotboom DJ (2015) Low Affinity and slow Na⁺-binding precedes high affinity aspartate binding in Glt_{ph}. *J Biol Chem* 290(26):15962–15972
37. Verdon G, Oh SC, Serio RN, Boudker O (2014) Coupled ion binding and structural transitions along the transport cycle of glutamate transporters. *eLife* 3:e02283
38. Alleva C, Kovalev K, Astashkin R, Berndt MI, Baeken C, Balandin T, Gordeliy V, Fahlke C, Machtens J-P (2020) Na⁺-dependent gate dynamics and electrostatic attraction ensure substrate coupling in glutamate transporters. *Sci Adv* 6(47):eaba9854
39. Riederer EA, Valiyaveetil FI (2019) Investigation of the allosteric coupling mechanism in a glutamate transporter homolog via unnatural amino acid mutagenesis. *Proc Natl Acad Sci USA* 116(32):15939–15946
40. Phillips JC, Braun R, Wang W, Gumbart J, Tajkhorshid E, Villa E, Chipot C, Skeel RD, Kalé L, Schulten K (2005) Scalable molecular dynamics with NAMD. *J Comput Chem* 26(16):1781–1802
41. Best RB, Zhu X, Shim J, Lopes PEM, Mittal J, Feig M, Mackerell Jr AD (2012) Optimization of the additive CHARMM All-Atom protein force field targeting improved sampling of the backbone ϕ , ψ and side-chain $\chi(1)$ and $\chi(2)$ dihedral angles. *J Chem Theory Comput* 8(9):3257–3273
42. Klauda JB, Venable RM, Alfredo Freites J, O'Connor JW, Tobias DJ, Mondragon-Ramirez C, Vorobyov I, MacKerell Jr AD, Pastor RW (2010) Update of the CHARMM all-atom additive force field for lipids: validation on six lipid types. *J Phys Chem B* 114(23):7830–7843
43. Darden T, York D, Pedersen L (1993) Particle mesh Ewald: an N·log(N) method for Ewald sums in large systems. *J Chem Phys* 98(12):10089–10092
44. Humphrey W, Dalke A, Schulten K (1996) VMD: visual molecular dynamics. *J Mol Graph* 14(1):33–38
45. Staritzbichler R, Anselmi C, Forrest LR, Faraldo-Gómez JD (2011) GRIFFIN: a versatile methodology for optimization of protein-lipid interfaces for membrane protein simulations. *J Chem Theory Comput* 7(4):1167–1176
46. Zhang L, Hermans J (1996) Hydrophilicity of cavities in proteins. *Proteins* 24(4):433–438
47. Arkhipova V, Trinco G, Ettema TW, Jensen S, Slotboom DJ, Guskov A (2019) Binding and transport of D-aspartate by the glutamate transporter homologue Glt_{TK}. *eLife* 8:e45286
48. Fitzgerald GA, Mulligan C, Mindell JA (2017) A general method for determining secondary active transporter substrate stoichiometry. *eLife* 6:e21016
49. Moon CP, Fleming KG (2011) Side-chain hydrophobicity scale derived from transmembrane protein folding into lipid bilayers. *Proc Natl Acad Sci USA* 108(25):10174–10177
50. Armstrong CT, Mason PE, Ross Anderson JL, Dempsey CE (2016) Arginine side chain interactions and the role of arginine as a gating charge carrier in voltage sensitive ion channels. *Sci Rep* 6:21759

51. Pal D, Chakrabarti P (2001) Non-hydrogen bond interactions involving the methionine sulfur atom. *J Biomol Struct Dyn* 19(1):115–128
52. Valley CC, Cembran A, Perlmutter JD, Lewis AK, Labello NP, Gao J, Sachs JN (2012) The methionine-aromatic motif plays a unique role in stabilizing protein structure. *J Biol Chem* 287(42):34979–34991
53. Setiadi J, Kuyucak S (2017) Elucidation of the role of a conserved methionine in glutamate transporters and its implication for force fields. *J Phys Chem B* 121(41):9526–9531
54. DeChancie J, Shrivastava IH, Bahar I (2011) The mechanism of substrate release by the aspartate transporter Glt_{ph}: insights from simulations. *Mol BioSyst* 7(3):832–842
55. Venkatesan S, Saha K, Sohail A, Sandtner W, Freissmuth M, Ecker GF, Sitte HH, Stockner T (2015) Refinement of the central steps of substrate transport by the aspartate transporter Glt_{ph}: elucidating the role of the Na₂ sodium binding site. *PLoS Comput Biol* 11(10):e1004551
56. Zomot E, Bahar I (2013) Intracellular gating in an inward-facing state of aspartate transporter Glt(Ph) is regulated by the movements of the helical hairpin HP2. *J Biol Chem* 288(12):8231–8237
57. Oh S, Boudker O (2018) Kinetic mechanism of coupled binding in sodium-aspartate symporter Glt_{ph}. *eLife* 7:e37291
58. Bernèche S, Roux B (2001) Energetics of ion conduction through the K⁺ channel. *Nature* 414(6859):73–77
59. Liao J, Marinelli F, Lee C, Huang Y, Faraldo-Gómez JD, Jiang Y (2016) Mechanism of extracellular ion exchange and binding-site occlusion in a sodium/calcium exchanger. *Nat Struct Mol Biol* 23(6):590–599
60. Luo Y, Roux B (2010) Simulation of osmotic pressure in concentrated aqueous salt solutions. *J Phys Chem Lett* 1(1):183–189
61. Venable RM, Luo Y, Gawrisch K, Roux B, Pastor RW (2013) Simulations of anionic lipid membranes: development of interaction-specific ion parameters and validation using NMR data. *J Phys Chem B* 117(35):10183–10192
62. Reeves JP, Hale CC (1984) The stoichiometry of the cardiac sodium-calcium exchange system. *J Biol Chem* 259(12):7733–7739
63. Shlosman I, Marinelli F, Faraldo-Gómez JD, Mindell JA (2018) The prokaryotic Na⁺/Ca²⁺ exchanger NCX_{Mj} transports Na⁺ and Ca²⁺ in a 3:1 stoichiometry. *J G Physiol* 150(1):51–65
64. Harding MM, Nowicki MW, Walkinshaw MD (2010) Metals in protein structures: a review of their principal features. *Crystallogr Rev* 16(4):247–302
65. Kortzak D, Alleva C, Weyand I, Ewers D, Zimmermann MI, Franzen A, Machtens J-P, Fahlke C (2019) Allosteric gate modulation confers K⁺ coupling in glutamate transporters. *The EMBO Journal* 38(19):e101468

Publisher's Note Springer Nature remains neutral with regard to jurisdictional claims in published maps and institutional affiliations.